Density waves in shear-thickening suspensions

Guillaume Ovarlez, Anh Vu Nguyen Le, Wilbert Smit, Abdoulaye Fall, Romain Mari, Guillaume Chatté, Annie Colin

CONDENSED MATTER PHYSICS

Density waves in shear-thickening suspensions

Guillaume Ovarlez[1]*, Anh Vu Nguyen Le[2†], Wilbert J. Smit[2†], Abdoulaye Fall[3†], Romain Mari[4†], Guillaume Chatté[5†], Annie Colin[2]*

Shear thickening corresponds to an increase of the viscosity as a function of the shear rate. It is observed in many concentrated suspensions in nature and industry: water or oil saturated sediments, crystal-bearing magma, fresh concrete, silica suspensions, and cornstarch mixtures. Here, we reveal how shear-thickening suspensions flow, shedding light onto as yet non-understood complex dynamics reported in the literature. When shear thickening is important, we show the existence of density fluctuations that appear as periodic waves moving in the direction of flow and breaking azimuthal symmetry. They come with strong normal stress fluctuations of the same periodicity. The flow includes small areas of normal stresses of the order of tens of kilopascals and areas of normal stresses of the order of hundreds of pascals. These stress inhomogeneities could play an important role in the damage caused by thickening fluids in the industry.

INTRODUCTION

Complex fluids, such as gels, emulsions, polymers, granular media, and suspensions, are multiphasic materials characterized by a nonlinear macroscopic behavior (*1*), which is central in their use. For example, the shear thinning (decrease of viscosity with the shear rate) promotes the pumping of complex fluids; the yield stress (below which they have a solid-like behavior) of concentrated emulsions favors their use in stable cosmetic creams. Shear thickening, which corresponds to an increase of the viscosity as a function of the shear rate (*2*), is observed in many concentrated suspensions in nature and industry (*3*): water or oil saturated sediments, muds, crystal-bearing magma, fresh concrete, silica suspensions, corn flour mixtures, and latex suspensions. Industrially, this can have disastrous effects by damaging mixer blades or clogging pipes.

Although their compositions are diverse, complex fluids all have a structure characterized by a mesoscopic size (*1*). Flow-structure coupling then leads to their non-Newtonian behavior, as well as to original instabilities occurring at low Reynolds number (*1*). They have thus aroused the physicists' interest as fascinating systems to study phase transitions (*4*). When the characteristic time of the flow is smaller than the characteristic structural relaxation time of the material, a phase with a new structure is created. This shear-induced phase usually has a different viscosity than the material quiescent phase. Under homogeneous drive, there are conditions in which both phases can coexist adjacent in space at the same time, and inhomogeneous flow is expected.

For shear-thinning materials, such as colloidal gels and wormlike micelles, the situation is well documented (*5*). Colloidal gels can either be a solid-like percolated particle network or a liquid-like suspension of independent aggregates (*6*). Wormlike micelles at rest are in an isotropic phase and can transition to a nematic phase under shear (*7*). The signature of the shear-induced transition is a stress plateau in the shear stress versus shear rate flow curve. When the macroscopic shear rate (typically defined between two infinite plates as the ratio between the plates relative velocity and the distance between them) is imposed in a homogeneous stress field, this comes with a shear-banding transition: two layers of different shear rates oriented along the flow gradient coexist (*8*), with a relative size tuned by the value of the macroscopic shear rate. In some cases, this banded flow becomes unstable toward perturbations in the vorticity direction, giving rise to complex spatiotemporal response, although this might not correspond to phase transitions in the vorticity direction (*9*).

For non-Brownian shear-thickening suspensions, the description of the dynamics and of the structure of the flow during the shear-thickening transition is still unknown. As regard the structural transition experienced by the material, it has only recently been elucidated and described as a transition between lubricated and frictional particle contacts. If short-range repulsive forces exist between the particles, the contacts are lubricated at low shear rate. At high shear rate, high normal stresses are developed, the repulsive forces are overcome, and the contacts are frictional leading to an increase of the viscosity (*10*–*18*). When strong, this effect creates a discontinuous transition that comes with complex temporal fluctuations of the macroscopic shear rate under constant applied shear stress (*19*). The signature of discontinuous shear thickening (DST) is a constant shear rate (i.e., a vertical plateau) in the shear stress versus shear rate flow curve, which contrasts with the case of micellar solutions and colloidal gels. Previously unknown flow inhomogeneities are then expected theoretically to develop. At imposed macroscopic shear stress, the system should separate into bands of different stress (but same shear rate) in the vorticity direction or of different solid fraction in the gradient direction. However, normal stress balance across the interface between bands prevents the existence of steady bands (*19*). By combining the Wyart-Cates model for the shear-thickening transition (*12*) and a suspension balance model for the particle migration, a recent theoretical and numerical study points out the possible existence of long-lived unsteady bands in the vorticity direction (*20*); such bands would be characterized by both different stresses and densities and would travel along the vorticity direction.

At this stage, there exists no direct experimental evidence of these bands and of their dynamics: signs of their possible existence are fluctuating inhomogeneities of stress (*21*) and of velocity (*22*). This mainly comes from the difficulty to measure the temporal and the spatial

[1]Univ. Bordeaux, CNRS, Solvay, LOF, UMR 5258, F-33608 Pessac, France. [2]ESPCI Paris, PSL Research University, MIE-CBI, CNRS UMR 8231, 10, Rue Vauquelin, F-75231 Paris Cedex 05, France. [3]Univ. Paris Est, Laboratoire Navier, UMR 8205 CNRS - Ecole des Ponts ParisTech – IFSTTAR 5 bd Descartes, 77454 Marne-la-Vallée Cedex 2, France. [4]Univ. Grenoble Alpes, CNRS, LIPHY, F-38000 Grenoble, France. [5]ESPCI Paris, PSL Research University, SIMM, CNRS UMR 7615, 10, Rue Vauquelin, F-75231 Paris Cedex 05, France.
*Corresponding author. Email: annie.colin@espci.fr (A.C.); guillaume.ovarlez@u-bordeaux.fr (G.O.)
†These authors contributed equally to this work.

evolution of local variables such as solid-fraction profiles with high resolution. Here, we make a major advance in understanding this problem thanks to a novel combination of state-of-the-art x-ray radiography with rheological measurements (*23*). In contrast to previous studies, this experimental setup allows us to provide a clear view of the dynamics of the flow by getting a direct visualization of the solid-fraction map.

We study two well-known shear-thickening suspensions: a cornstarch suspension in water and salt (*3*, *19*, *22*, *24*, *25*) and monodisperse suspension of polyvinyl chloride (PVC) particles in a Newtonian solvent (Dinch) (*17*, *26*, *27*). We show that the behavior of these samples displays generic features. We find that inhomogeneities occur in the flow direction in the form of density waves. Our data shed new light onto yet non-understood interfacial instabilities and viscosity fluctuations and pave the road for future theoretical works.

RESULTS

PVC suspension: A canonical system

We first focus on PVC particles dispersed in liquid Dinch (1,2-cyclohexane dicarboxylic acid diisononyl ester). The continuous phase is Newtonian up to a shear rate of 10^{ν} s^{-1} and has a viscosity of 41 mPa·s at room temperature (*27*). Dinch is an organic solvent that acts as a plasticizer for the particles. It enters the particles, creates a polymer brush around them, and eventually completely swells them. Far below the glass transition temperature of PVC (T_g = 80°C), this process is extremely slow. At room temperature, it takes more than 1 year: Dinch then swells only the particle surface on a few nanometers [experimentally measured in (*17*)], creating a swelled PVC brush layer at the particle surface that sterically stabilizes our suspensions (*28*). The mean particle radius is 1 μm and their root mean square (RMS) roughness is 2.2 nm. The size distribution is log-normal, and the SD estimated using the volume distribution is 45%. Further details on the particle characteristics and on the suspension macroscopic properties can be found in (*17*, *27*) and in Materials and Methods. In this work, we focus on a suspension with a volume fraction of 60%. We first measure the rheological properties using a thin-gap sandblasted Couette cell with a rotor radius of 28 mm and a gap of 1.2 mm at 25°C. The macroscopic shear rate $\dot{\gamma}$ is obtained under constant imposed stress ramped up from 1 to 500 Pa in 36 logarithmically spaced steps of 60 s. As shown in Fig. 1 (E and F), the suspension exhibits a slight shear-thinning behavior at low shear stress and a shear-thickening behavior above the critical shear stress $\sigma_c \simeq 145$ Pa.

The shear-thinning behavior at low shear stress has been discussed in detail in (*27*). It was shown that this suspension does not present any slip in both its thinning and thickening regimes. At low shear stress, the PVC suspension behaves as a hard spheres suspension with an apparent size that includes the hard radius and a part of the surrounding soft repulsive potential which varies as a function of the shear rate. Such thinning has already been observed in a charge stabilized suspension (*29*, *30*) and predicted numerically (*13*). The shear-thickening behavior can be explained following (*12*). Previously, we have characterized the interactions between pairs of PVC particles using a tuning fork (*17*). We have found that the critical shear stress σ_c at the shear-thickening transition is tuned by the repulsive force due to the brush layer at the particle surface. The discontinuous shear-thickening transition is thus unambiguously explained by the breakdown of lubrication between particles and the onset of hard frictional contacts. Consistently, we have shown that the solid fraction at which the zero shear rate viscosity diverges is equal to the random close packing ϕ_{rcp} = 69%, thus corresponding to a frictionless state, and that the solid fraction at which the high shear rate viscosity diverges is ϕ_m = 62%, corresponding to the frictional state (*27*). These observations are in excellent agreement with the model developed by Wyart and Cates (*12*) and with numerical simulations of Mari *et al.* (*13*). This suspension can then be seen as a canonical system: The in-depth study of its dynamics is thus a crucial test for the current understanding of dense suspensions.

Shear rate fluctuations

Next, we focus on the dynamical behavior of the suspension. To do so, after the stress ramp, we impose various constant shear stresses (50, 133, 200, and 270 Pa) during long steps of at least 3600 s each (see Fig. 1, A to D). Averages of the resulting macroscopic shear rate $\dot{\gamma}(t)$ over the last 1800 s of each step are plotted in Fig. 1 (E and F). Note that they do not perfectly coincide with the previously measured flow curve, notably in the shear-thickening region: The apparent behavior depends upon the shear history of the sample, which will be commented at the end of the article.

In Fig. 1 (A to D), we show a portion of the shear-rate time traces. Below σ_c, the fluctuations are negligible (less than 0.2%) with a periodicity corresponding to one revolution of the rotor, pointing to unavoidable slight geometrical imperfections of the Couette cell or of the torque mapping of the rheometer. Above σ_c, the macroscopic shear rate exhibits periodic fluctuations of high amplitude (of order 10%) as often observed in thickening systems (*19*), which are statistically stationary. Note that these oscillations are smooth and are not due to inertia oscillations of the rotor, in contrast to stick-slip oscillations observed by others (*31*, *32*). Here, the torque due to inertia is found to be always at least 40 times smaller than the torque due to the material resistance to flow. The periodicity of the fluctuations in the thickening regime now corresponds roughly to two revolutions of the rotor, i.e., on average, to one revolution of the convected suspension in the gap of the cell.

This readily suggests that the azimuthal symmetry of the flow is broken, as will be proved and discussed below.

To better understand this point, we position the cup of the Couette cell on two horizontal translation stages so as to precisely position the axis of the stator with respect to the rotor axis, and we willingly play with eccentricity. Figure 1G shows the temporal evolution of the shear rate obtained as a function of the eccentricity of the cell when a shear stress of 200 Pa is applied. The amplitude of the fluctuations strongly varies with the eccentricity. A distance of 50 μm between the rotor and stator axes is enough to double the fluctuation amplitude (without changing its period). These data evidence a direct coupling of the internal dynamics and the geometry and suggest symmetry breaking of the suspension flowing properties. In the following, the value of the eccentricity will be less than 10 μm, which is the maximum mechanical accuracy achievable.

X-ray imaging

The rheological behavior of suspensions depends upon the solid fraction. To probe whether the rheological fluctuations come with fluctuations of the solid fraction, we use a Phoenix v|tome|x s from General Electric in two-dimensional (2D) mode and make radiography of spatial x-ray absorption. The experimental setup and the measurements methods are detailed in (*23*). An x-ray planar wave is penetrating a Couette cell made of poly(methyl methacrylate) (PMMA). The x-rays

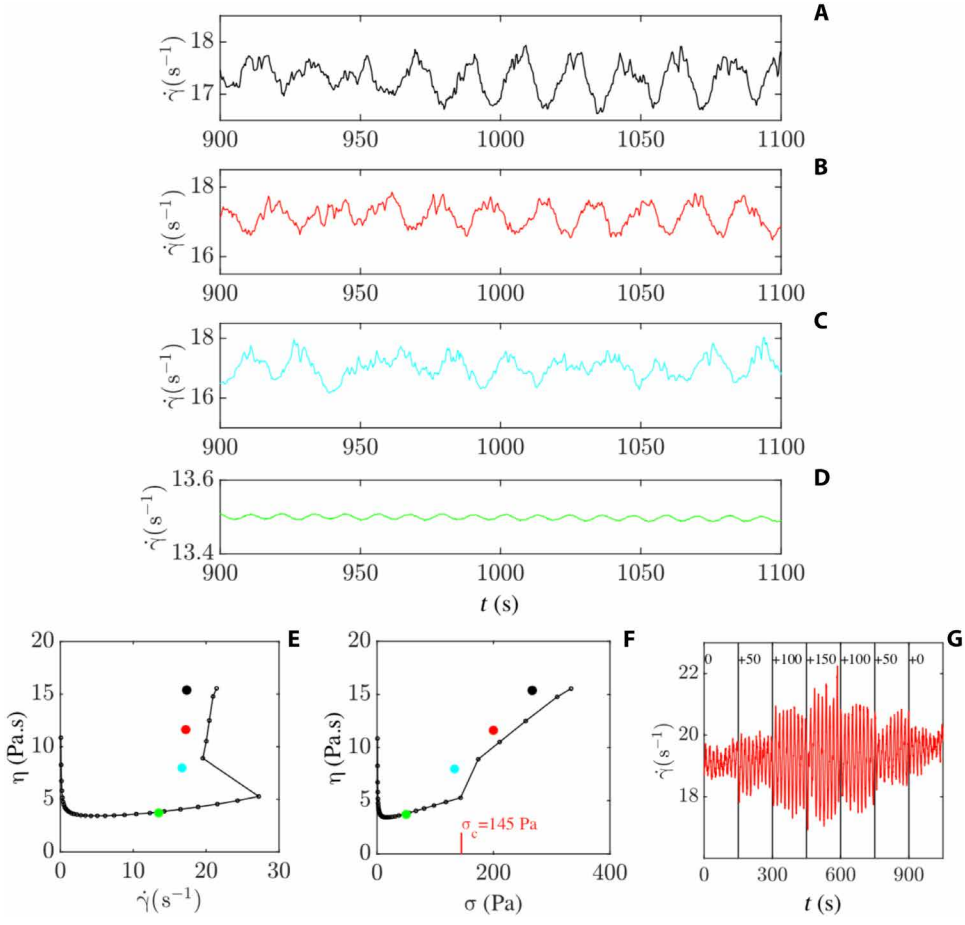

Fig. 1. PVC suspension (60%) in Dinch. (**A** to **D**) Portions of the time traces of the macroscopic shear rate under constant shear stress. See section S1 for the signals over 1800 s. The applied shear stress in the peak hold stress experiments are: 270 Pa (A, black), 200 Pa (B, red), 133 Pa (C, cyan), and 50 Pa (D, green). In a Couette cell, the measured average shear rate and the period T_{rot} of the motor are linked by $\frac{1}{T_{rot}} = \frac{R_o^2 - R_i^2}{R_o^2 + R_i^2} \frac{\dot{\gamma}}{2\pi}$, where R_o is the stator radius and R_i is the rotor radius ($R_o = R_i - e$). In our case, this leads to T_{rot} = 8.8 s for a macroscopic shear rate of 17 s^{-1} and to T_{rot} = 11 s for a macroscopic shear rate of 13.5 s^{-1}. Above the shear thickening transition, large oscillations are observed with a period roughly equal to 18 s for (A) to (C), i.e., two times that of the rotor period rotation (T_{rot}= 8.8 s). Below the shear-thickening transition, the oscillation has a much smaller amplitude and their period is equal to the rotor period rotation, i.e., 11 s. (**E**) Variation of the apparent viscosity as function of the shear rate recorded in a Couette geometry by ramping up the imposed stress with 60 s per point (small empty black circles) and through subsequent constant stress experiments of at least 3600 s (filled colored circles; shear rate is averaged over the last 2500 s of each step). (**F**) Same as (E), viscosity as a function of the shear stress. (**G**) Effect of the eccentricity (indicated above the curve, in μm; steps of 150 s) of the Couette cell on the dynamics. The applied shear stress is 200 Pa.

are partially absorbed by the various media crossed by the beam (PMMA, PVC particles, Dinch, air, and water in the cooling system) obeying the Beer-Lambert law.

The normalized solid fraction $\widetilde{\Phi}$ seen by the beam in the Couette cell is linked to the recorded x-ray intensity I by

$$\widetilde{\Phi}(y,z,t) \equiv \frac{\Phi(y,z,t)}{\Phi_0(y,z)} = \frac{\ln\left[I(y,z,t)/I_{solvent}(y,z)\right]}{\ln\left[I_0(y,z)/I_{solvent}(y,z)\right]} \quad (1)$$

where y is the horizontal direction on the x-ray detector, z is the vertical direction (corresponding to the vorticity direction), $I_{solvent}$ is the recorded intensity in the absence of particles (i.e., liquid Dinch alone), and subscript 0 denotes the initial static values. Note that x-ray radiography is the 2D projection of a 3D object on a detector, which is an attenuation map averaged over the object thickness. The measured solid fraction $\Phi(y, z, t)$ is an average over a varying thickness x depending on y (see the red zone on Fig. 2A). Here, images are obtained with a pixel resolution corresponding to 25 μm.

Geometry and interface fluctuations

First, we use x-ray imaging to characterize the geometry and to measure the position of the rotor and of the stator as a function of time. We performed these experiments in a Couette cell with a rotor radius equal to 24 mm and a gap of 1 mm. Both measurements are obtained by tracking the average position of the walls more than 20 pixels located at the top of the cylinders along the z direction. Below the shear-thickening transition, the rotor and the stator are concentric and rotate with no observable fluctuations. Above the shear-thickening transition, the position of the rotor fluctuates with time (Fig. 2C), whereas the stator does not move. This means that strong stress inhomogeneities are developed along the flow direction, leading to a neat off-axis force bending the rheometer axis. As for the macroscopic oscillations in the shear rate, the angular period of these fluctuations correspond to two revolutions of the rotor. The x-ray method has a temporal resolution of 0.2 s. We underline that displacement of the rotor does not affect the solid-fraction measurements. As long as the stator does not move, which is the case in our study, the scattering volume is constant

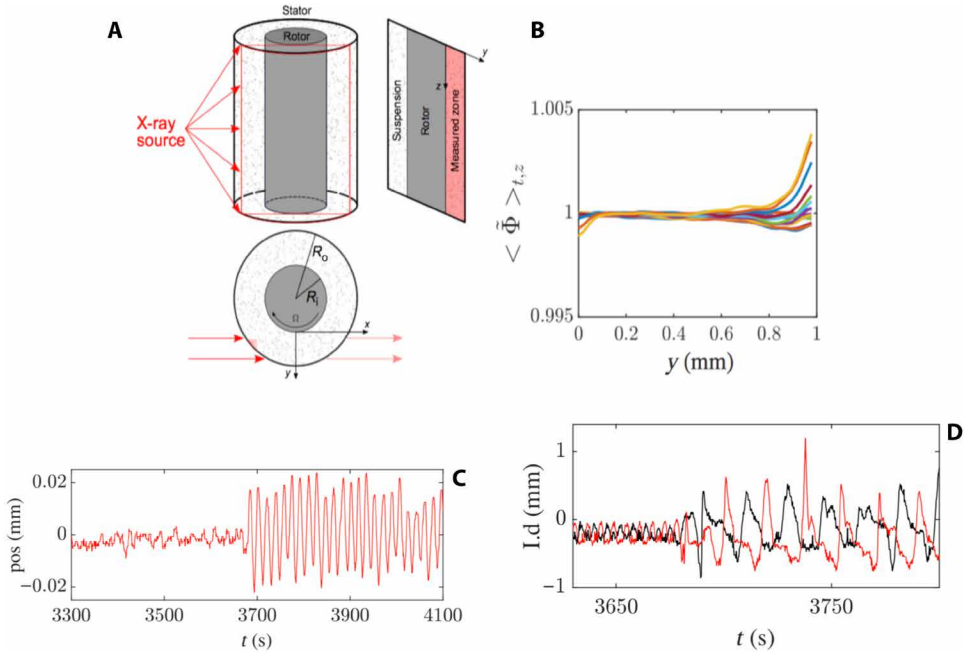

Fig. 2. PVC suspension (60%) in Dinch. (**A**) Scheme of the x-ray setup. The *y* direction is the horizontal direction on the x-ray detector. The *z* direction is the vertical direction and corresponds to the axis of the rotor. (**B**) Normalized solid fraction averaged over time and vertical position, $\langle\widetilde{\Phi}\rangle_{t,z}(y)$, as a function of the position in the gap *y* for various shear stresses. (**C**) Variation of the horizontal position (pos) in millimeters of the rotor as a function of time (for $t < 3660$ s the applied shear stress σ is 125 Pa, for $t > 3660$ s, σ = 150 Pa and the system is in the shear-thickening regime); the rotor remains centered below the shear-thickening transition and oscillates above. (**D**) Vertical displacement of the air/sample interface (l.d) as a function of time for the same stresses as in (C); the red curve corresponds to the Couette cell gap imaged on the left side of the detector (see Fig. 2A), and the black curve to the gap imaged on the right side of the detector. For σ = 125 Pa, the rotation velocity of the rotor is Ω = 1.02 rad/s; for σ = 150 Pa, Ω = 0.72 rad/s. The period of the waves is equal to 18 s and is two times the period of the rotor (equal to 8.7 s) for both (B) and (C).

and our analysis is relevant. Using x-ray imaging, we also track the position of the air/suspension interface as a function of time. Figure 2D displays the position of the interface as a function of time in two opposite locations of the gap. Below the shear-thickening transition, the interface does not move and remains flat. Above the shear-thickening transition, they oscillate in phase opposition in both parts of the Couette cell. The amplitude of the oscillations is large and may reach 2 mm. These data are in agreement with macroscopic observations of the interface in a wide-gap cell (see section S2). Assuming that there is a single front (which is verified by macroscopic observations), we can measure the velocity of the wave V_{wave}. We observe that $V_{\text{wave}} \simeq \frac{\Omega R}{2}$ over the entire shear-thickening transition. In other words, the angular periodicity of these interface fluctuations corresponds to two revolutions of the rotor, which is correlated with the rotor position oscillations and with the macroscopic shear rate fluctuations. This will be analyzed in more detail below.

Density fluctuations

Second, we use x-ray absorption to map the solid-fraction profiles. Figure 2B displays profiles of the solid fraction averaged over time and vertical position, $\langle\widetilde{\Phi}\rangle_{t,z}(y)$, as a function of the position in the gap *y* for various shear stress. These data are time-averaged over the entire peak hold stress and spatially averaged over the height of the Couette cell. The solid fraction remains constant and homogeneous below the shear-thickening transition (see Fig. 3A for a map in the *y*, *z* plane). At high shear stress in the shear-thickening regime (i.e., above $\sigma_c \simeq$ 150 Pa), a slight increase in solid fraction is observed only very close to the stator, showing that shear-induced radial migration occurs. Its magnitude ($\Delta\Phi/\Phi < 0.2\%$) in our thin-gap Couette geometry is consistent with interpolation that can be made from the typical magnitude observed in a wide-gap Couette geometry with concentrated suspensions (*23*, *33*). Although we did not use exactly the same procedure in Fig. 1, we believe that this slight radial migration is at the origin of the dependence on the history of the sample mentioned above. Starting from a fresh sample involves a homogeneous sample. Performing a peak hold after a ramp involves a slightly inhomogeneous sample.

We then focus on the evolution of the solid fraction in the flow direction. Since our measurement zone is fixed, studying the temporal fluctuations of $\widetilde{\Phi}(y,z,t)$ is equivalent to studying density variations in the flow direction.

Figure 3 (A to D) displays instantaneous solid fraction maps in the *y*, *z* detection plane, for an applied shear stress of 200 Pa, above the shear-thickening transition. These maps evidence large periodic temporal fluctuations of the density, with relative variation of order 10%, mainly located at the top of the sample. Some zones display solid fraction higher than 66% and even very close to 69%. Recalling that $\phi_m = 62\%$ and $\phi_{RCP} = 69\%$ (*27*), the system is thus shear-jammed in these inhomogeneities.

Note that the lowest values of the measured density are the signature of a periodic introduction of air in the sample, which is due to the free interface fluctuations (*34*). Figure 3E displays the temporal evolution of the gap-averaged solid fraction, together with that of the viscosity, the rotor displacement, and the free interface displacement. As shown in the section S4, all signals display the same main frequency (0.06 Hz), which is two times

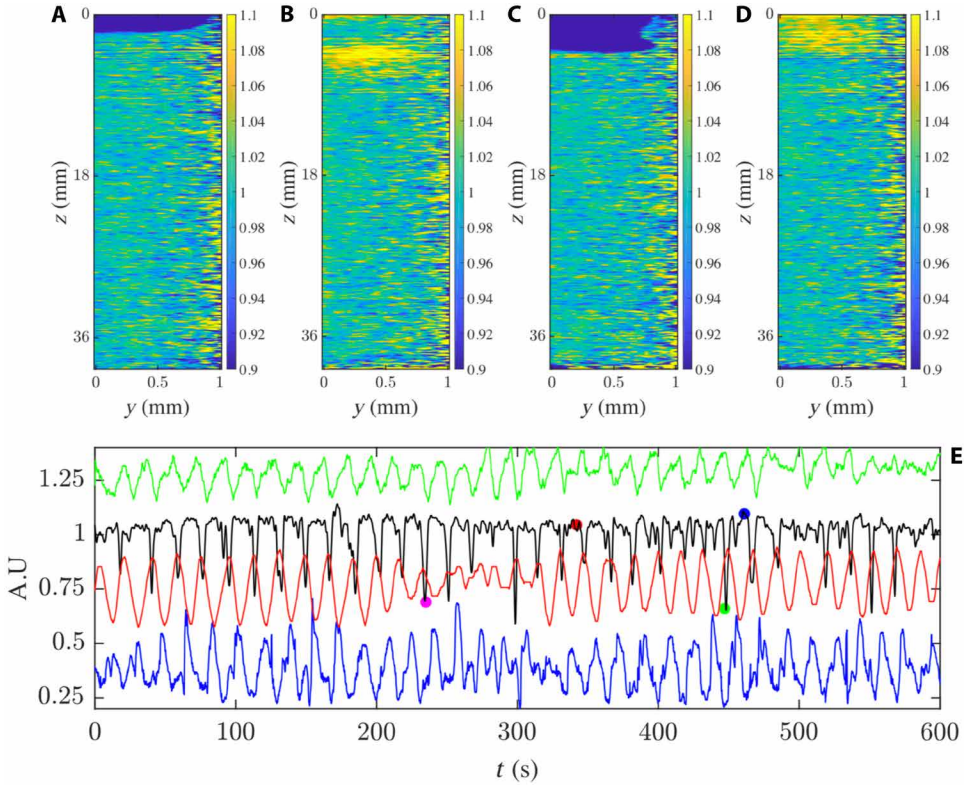

Fig. 3. PVC (60%) suspension in Dinch. (**A**) Instantaneous map of the solid fraction corresponding to the pink circle in (E). (**B**) Same as (A) for the red circle in (E). (**C**) Same as (A) for the green circle in (E). (**D**) Same as (A) for the blue circle in (E). (**E**) From top to bottom, temporal evolution of the normalized macroscopic shear rate $\dot{\gamma}_N = \dot{\gamma}/10 - 0.7$ (green line), of the solid fraction $\langle\overline{\Phi}\rangle$ (black line), of the normalized rotor displacement $d_N^R = d^R \times 6.89 + 0.75$, where d^R is the displacement of the rotor expressed in millimeters (red line), of the normalized interface position $lp_N = lp/5 + 0.4$, where lp is the interface displacement expressed in millimeters (right part of the cell Couette, blue line). The solid fraction $\langle\overline{\Phi}\rangle$ is the instantaneous solid fraction averaged over the entire gap along the *y* direction and more than 1 cm below the free interface in the *z* direction. The data corresponding to the positions at a distance less than 100 μm from the rotor and 100 μm from the stator are excluded. A.U., arbitrary units.

smaller than that of the motor (0.13 Hz): It corresponds to the average convection velocity of the material.

The solid fraction and the rotor displacement are in phase opposition, i.e., the larger the solid fraction, the larger the gap width. The zones of high density thus exert a high positive normal stress on the rotor surface, which causes its displacement. As normal stresses are usually proportional to shear stresses in such systems, we can also conclude that these zones bear high shear stresses. High solid fraction thus corresponds to high viscosity. The signal of the interface position is in phase with the solid fraction but in phase opposition with the rotor displacement. The shear rate signal has the same frequency as the other signals. Figure S3 shows a similar behavior for applied shear stresses of 150 and 300 Pa. At the opposite, no variations are measured for a shear stress equal to 125 Pa, below the shear-thickening transition.

A clear picture of the flow lastly emerges from our data. As time is linked to the flow direction through advection, it follows that the shear-thickening transition is associated with particle density waves located mainly at the top of the Couette cell and advancing along the flow direction. These density waves encompass shear-jammed zones. They come with strong stress fluctuations yielding an off-axis movement of the rotor and with an interfacial instability: A surface wave propagates with a velocity equal to half the rotor velocity, and air is also introduced periodically at the top of the sample. Apparent shear rate (and thus, viscosity) fluctuations are lastly induced and are due to the interplay between the axial symmetry breaking and the imperfect concentricity of the Couette cell. Note that the shear rate seems to be in phase with the solid fraction. It is impossible, however, to analyze the phase between these two signals. The measured shear rate is a macroscopic quantity and is low when the most viscous part of the sample is located in the thinnest part of the Couette gap. By contrast, the density is a local value measured at a fixed location, and we do not know whether it corresponds to the thinnest part of the gap or not. The previous analysis made using the normal stresses points out that the high-density zones are correlated to high viscosity, which suggests that local data are not collected at the thinnest gap location.

To estimate the stress applied by the density inhomogeneities on the rotor, we have measured the lateral stiffness of the rotor, by measuring the force exerted to move the rotor with a rigid tip of small contact area positioned at the same location as the observed density inhomogeneity. This stiffness is equal to 1.5×10^4 N m^{-1}. On the basis of the x-ray measurements, we estimate that the inhomogeneity covers a region of 3 mm in height and of length equal to 1/20 of the rotor perimeter. This length is estimated by counting the fraction of images per revolution where the inhomogeneity is observed.

Assuming that this inhomogeneity is characterized by a large normal stress causing the rotor displacement, we can then estimate this normal stress to be of the order of 30 kPa in the PVC suspension when the average applied shear stress is 150 Pa, which is consistent

with the stress values observed by (*27*), using capillary rheometry, on the same system in its frictional state (i.e., corresponding to the maximum measured viscosity).

The flow thus includes small areas of normal stresses of the order of tens of kilopascals as well as areas of normal stress of the order of hundreds of pascals. We believe that these strong stress variations could play an important role in the damage caused by thickening fluids in the industry.

It is interesting to ask whether the shear-thickening suspensions we are studying are subject to dilatancy or not. To do this, it is necessary to compare the lower bound of the confinement pressure P_{conf} that can be calculated according to Cates from the surface tension γ and grain size a, $P_{conf} = \frac{2\gamma}{a}$, and the typical stress previously estimated in the dense regions. We find P_{conf} = 100 kPa for PVC suspension using a radius of 1 μm and a surface tension of 50 mN/m. The stress inside the inhomogeneities is 30% less than the confinement pressure. This is the first argument to indicate that the samples do not experience dilatancy, although the values are not so different. This conclusion is reinforced by the fact the interfaces of the samples submitted to shear remain shiny (see, for example, fig. S2). The interface of a system subject to dilatancy is rough and scatters light, which we do not observe.

Density waves in cornstarch

To conclude this experimental section, we extend this study to another suspension. We repeat the measurements for a cornstarch suspension in salty water. The cornstarch is supplied by Merck (CAS 9005-25-8) and used without further modification. It contains approximately 73% amylopectin and 27% amylose with a particle diameter of 14 μm (with a polydispersity of 40% as determined from static light scattering). Salt is used to match the density and to enhance the x-ray contrast. Dense cornstarch suspensions are obtained by dispersing 41 wt % of cornstarch at room temperature in a density-matched solvent composed of 46 wt % water and 54 wt % cesium chloride (CsCl). We measured the rheological properties by applying peak hold stresses (see figure legends for the applied values). Cornstarch suspensions are known to exhibit slip at the wall. We thus study the suspensions in both smooth and rough geometry. The flow curves are given in sections S5 and S6: Shear thinning is observed at low shear stresses, a continuous shear-thickening regime is then observed for stresses higher than 1 Pa, whereas a transition to a discontinuous shear-thickening regime is observed above 6 Pa. Figure 4 displays the density profiles for a smooth thin-gap Couette cell with a small gap of 0.5 mm and an internal radius of 24.5 mm. The case of rough surfaces is shown in section S6. We again observe spatial and temporal fluctuations of the solid-fraction profiles in the DST regime, similar to the case of PVC in Dinch.

Figure 4A first shows the solid fraction averaged close to the stator $\langle\widetilde{\Phi}\rangle_{stator(t)}$, as a function of time. These data are averaged over 40 μm next to the stator and over 2 cm below the free interface in the z direction; averaging only close to the stator allows to evidence both radial migration and time fluctuations in a unique plot. We first note a rapid and significant global increase in the solid fraction close to the rotor for stresses higher than 1 Pa, meaning that shear-induced radial migration occurs. We observe this behavior in the continuous shear-thickening regime, where radial migration has already been reported to be accelerated (*33*). We note that migration is much more important than in PVC suspensions and of much higher magnitude than expected in the thin-gap Couette used here: A density variation $\Delta\Phi/\Phi$ of order 3% is observed, whereas $\Delta\Phi/\Phi \simeq 0.1\%$ would be expected here from interpolation of typical migration profiles observed in wide-gap Couette geometries in concentrated suspensions (*33*). This might be due to the attractive forces between cornstarch particles and to the formation of a shear-induced consolidated gel. Hysteretic force profiles between cornstarch particles have been measured using atomic force microscopy (AFM) (*35*), evidencing attractive forces when the particles are separated after contact, which is not the case for PVC particles (*17*).

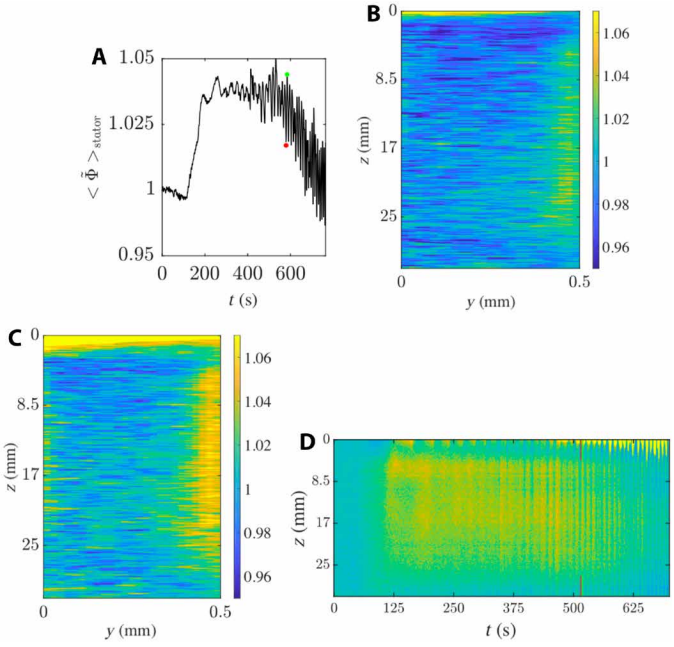

Fig. 4. Cornstarch suspension in CsCl solution in a smooth Couette geometry. We apply a series of constant shear stresses for 50 s each. The applied values are 0.3, 1, 2, 3, 5, 8, 10, 12, 15, 20, 25, 30, 40, and 60 Pa. Continuous shear thickening is observed for stresses above 1 Pa, and DST is observed for stresses above 6 Pa (see section S6). (**A**) Averaged normalized solid-fraction profile along z and y, $\langle\widetilde{\Phi}\rangle_{stator}$, as a function of time. These data are averaged over 40 μm close to the stator and over 2 cm below the free interface in the z direction. The green circle corresponds to t = 515 s, the red one to t = 520 s, for an applied shearstress equal to 25 Pa in the DST regime. (**B** and **C**) Instantaneous normalized solid-fraction maps $\widetilde{\Phi}(y,z,t)$. The applied shear stress is equal to 25 Pa, in the DST regime, at t = 515 s and t = 520 s for (B) and (C), respectively. The rheological data can be found in section S6. (**D**) Normalized solid fraction profile averaged over a width of 40 μm next to the stator, $\langle\widetilde{\Phi}\rangle_{stator}$, plotted as a function of time and height. The red tick corresponds to t = 515 s and the green one to t = 520 s, for an applied shear stress equal to 25 Pa in the DST regime.

It implies that cornstarch suspensions are not canonical systems that can be directly compared to the most recent theories and simulations (*12*, *13*): Although we expect them to present qualitatively the same behavior as other discontinuous shear-thickening suspensions, they display additional complex features and can be expected to present quantitative differences.

For stresses exceeding 6 Pa, corresponding to the onset of discontinuous shear thickening, we observe temporal fluctuations of the concentration. Instantaneous 2D maps corresponding, respectively, to a minimum and a maximum of these fluctuations are shown in Fig. 4 (B and C) and show that the whole 2D structure is involved in the fluctuations. As already pointed out, such solid-fraction

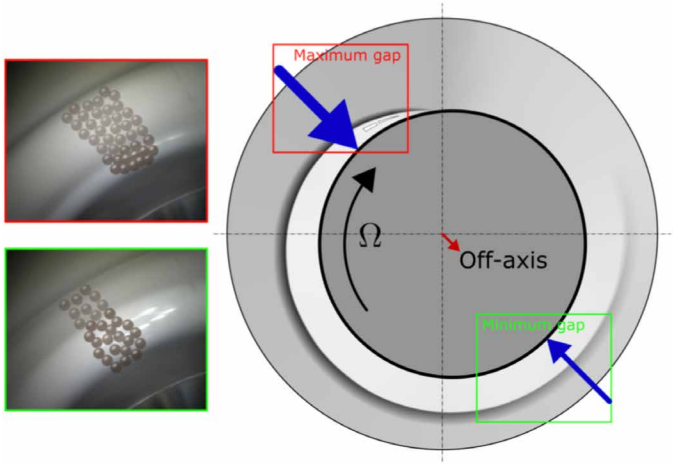

Fig. 5. Illustration of the mechanism in charge of the flow. A dense zone is created in one part of the rotor, resulting in a higher normal stress and thus with an unbalanced normal stress around the rotor. This induces a displacement of the rotor and creates a wave at the free interface. Apparent viscosity fluctuations in time result from the interplay between the axial symmetry breaking and the imperfect concentricity of the Couette cell.

fluctuations measured in a fixed zone correspond to fluctuations propagating in the velocity direction, as for PVC suspensions. The variations observed at the top surface are the signature of free-surface fluctuations as in PVC; this is also related to an off-axis motion of the rotor, evidencing stress fluctuations. The density fluctuations in time are rather periodic and are correlated to the free-surface and rotor fluctuations (see section S5). We notice two differences between PVC and cornstarch suspensions. Figure 4B shows a spatiotemporal plot of the density close to the stator: It shows that, in contrast to PVC, the fluctuations occur simultaneously along the whole height. A quantitative difference with PVC also exists: Whereas for PVC, the period of the density fluctuations is equal to twice the period of the rotor, here, the fluctuation period is roughly equal to three times the period of the rotor. Since the rheological curve evidences slip at the wall, the apparent shear rates are higher than the bulk shear rates, which likely leads to overestimating the intrinsic dynamics of the band. However, for the same sample with rough boundaries (see section S6), we get the same picture, with even different quantitative features. Although it is difficult to extract a characteristic time in that situation, due to the complexity of the signals, it can be noted that the dynamics is still faster than in PVC and is even faster than in the smooth case, although the macroscopic shear rates are smaller. It can lastly be concluded that the phenomenology is the same in cornstarch as in PVC. We do observe density waves propagating in the flow direction characterized by high normal stresses yielding an off-axis movement of the rotor. However, we evidence different dynamics (i.e., the period of the waves is not twice that of the motor), likely linked to the complexity due to the occurrence of significant radial migration in cornstarch, in relation with the adhesive forces between cornstarch particles. We estimated that the rotor displacement is caused by normal stresses of the order of 3 kPa, when the average applied shear stress is 25 Pa, which, as for the PVC suspension, is consistent with the stress values observed on the same system in its frictional state (*24*). We checked that no dilatancy occurs in our system. As previously, we calculate P_{conf} = 20 kPa for the cornstarch suspension using a radius of 8 μm and a surface tension of 72 mN/m.

Our results on cornstarch differ from the ones obtained by Saint-Michel *et al.* (*22*). In their recent work, the authors have studied cornstarch suspensions with local velocity measurements. They observed complex dynamics and have suggested that their data evidence vorticity bands propagating in the vorticity direction. Our measurements show that density fluctuations along the velocity direction are accompanied with waves at the free interface, implying a complex 3D motion; this likely leads to the observation of periodic velocity fluctuations along the vorticity direction, as those reported in (*22*). Moreover, an experimental detail may be behind the difference between the two studies. To prevent evaporation, the authors have used a lid. In this situation, it is likely that they do not have a free interface but rather a flow confined between four walls. In a closed geometry, the wave of the free interface that we have observed may then generate in addition propagative events in the vorticity direction as the ones observed by Saint-Michel *et al.*

DISCUSSION

Our work points out that the discontinuous shear-thickening transition in a canonical system is associated with symmetry breaking in our Couette geometry, that is, with the breaking of invariance along the flow direction. On the basis of our observations, the following chain of events can then be reconstructed.

The discontinuous shear-thickening transition is accompanied by the coexistence of areas where interparticle contacts are frictional and areas where contacts are lubricated. These areas cannot stay organized in a stationary way in the flow, since the differences in normal stresses between these areas cause a particle migration from one area to the other. Here, we show that the flow is organized with a density wave that moves in the flow direction at a slower speed than the rotor. These solid fraction inhomogeneities withstand high stresses, which remain lower than the confinement pressure in our study. An indirect signature of the propagation of these inhomogeneities is the emergence of apparent viscosity fluctuations, which is due to unavoidable slight geometrical imperfections of the Couette cell. These macroscopic viscosity fluctuations are of much lower amplitude than the local fluctuations. If the flow geometry were not deformable, one would only observe these features.

In the case of a deformable geometry (case of any standard rheometer), the inhomogeneous normal stresses resulting from the inhomogeneous solid fraction distribution induce a displacement of the rotor. Top surface fluctuations then emerge as a consequence of the off-axis rotational movement.

The flow instability we have revealed seems to be generic for DST materials and to reconcile many observations of the literature. Our observations are consistent with the results obtained by Rathee *et al.* (*21*), who studied a suspension of submicronic silica beads in glycerol. These authors show that the shear stress field in their shear-thickening suspension is inhomogeneous in the thickening regime and that zones of high shear stresses propagate at half the velocity of the rotor along the velocity direction. Here, we shed new light on these observations by showing that this comes with solid-fraction density waves and high normal stresses. This conclusion likely applies too to the potato-starch suspension studied by Nagahiro and Nakanishi (*16*), who reported normal stress fluctuations traveling in the flow direction in the thickening regime. It also provides a possible

explanation for the rotor off-axis motion in the thickening regime, which had been previously reported for a latex suspension by (*36*), and for apparent viscosity fluctuations observed in many thickening systems, which has long remained an unanswered question (*19*). These results echo the pioneering work of Lootens *et al.* (*37*) where huge macroscopic shear stress fluctuations were reported between two states under applied shear rate in a thickening suspension. Note that the existence of aggregates was hypothesized by Lootens *et al.* (*37*) to explain these huge macroscopic fluctuations.

We lastly showed that the same phenomenology is observed with cornstarch suspensions, although it is more complex due to the interplay with strong shear-induced migration: We argue that cornstarch is far from being a canonical system due to the adhesion forces that are not present in the common framework adopted by the most recent simulations and theories (*12*, *13*).

At this stage, we are not able to determine unambiguously the nature of these solid fraction density waves from the experimental data. They may be either steady bands involving jammed zone or propagating density waves. A jammed zone could be transported by rolling between the two cylinders: Its convection velocity would then be half the rotor velocity as observed here. These bands would then correspond to the shear-jammed region of the phase diagram (*13*).

Propagating density waves and breaking of symmetry associated with DST is expected to occur under imposed shear stress, as opposed to imposed shear rate, as explained for instance in (*19*). Under imposed shear rate, the system is completely homogeneous, either in the low viscosity state at small rates (below the shear-thickening rate) or in the high viscosity state for large rate. Simulations under imposed stress are few (*20*, *38*). In wide systems, bands traveling in the vorticity direction have been predicted and observed in numerical simulations by Chacko *et al.* (*20*), which is due to the following mechanism. A local increase of stress induces a local increase of the number of frictional contacts. In the DST regime, any slight increase of the number of frictional contacts corresponds to a large increase in viscosity, so much so that it provides a positive feedback for stress fluctuations, and an instability. While this linear instability mechanism is a priori equally valid for wave vectors in both the velocity and vorticity directions, in the nonlinear, fully developed regime the two directions are not equivalent. For vorticity bands, the stress imbalance at the interface induces particle migration, which is a stabilizing process competing with the instability to give rise to permanent traveling bands, where the migration-thickening balance is achieved dynamically.

For velocity bands, however, the band interfaces are also subject to advection, a much more efficient transport mechanism than particle migration which is of diffusive nature. This may be why numerical simulations like the ones of (*20*) do not capture velocity bands. The simulations and modeling of (*20*) are assuming a setup with periodic boundary conditions, particularly in the vorticity direction. In the experiments, the free surface (in the vorticity direction) may prove a further positive feedback for stress fluctuations, counteracting advection by applying a permanent normal stress on the suspension in the velocity direction when the interface is wavy, as depicted in Fig. 3E. In this spirit, further works should deal with modeling these bands involving bulk thickening rheology and free-surface dynamics. We believe that these future works will be able to predict why velocity bands seem to be favored over vorticity bands. It may also provide insight as to the origin of instabilities observed in free-surface flows of shear-thickening suspensions (*39*).

By revealing an original flow instability in complex fluids, our experimental work opens the road to new models and simulations in the field of soft matter taking into account the possibility of breaking the invariance along the flow direction, which has never been considered before. These observations are also crucial for applications: The density waves are likely at the origin of damage occurring during pumping in industrial processes. It would now be interesting to see how it is possible to control these instabilities by adding vibrations perpendicular to the flow as recently proposed (*40*). The vibrations may avoid the density fluctuations and allow the control of the flow.

MATERIALS AND METHODS

PVC suspensions

The mean radius of PVC particles, defined as $R_{32} = \langle R^3 \rangle / \langle R^2 \rangle$ is 1 μm. Their RMS roughness measured by AFM is 2.2 nm. The size distribution is lognormal, and the SD estimated using the volume distribution is 45%. As a plasticizer for the PVC particles, we use *n*1,2-cyclohexane dicarboxyllic acid di-isonoly ester (Dinch) supplied by BASF. Dinch does not evaporate. The organic liquid Dinch enters the particles and creates a polymer brush around them. This brush enables suspension stabilization due to steric repulsion. At high temperature (T >100°C), Dinch can dissolve the PVC particles. At room temperature, this process is much slower and takes more than 1 year. Our measurements are performed 1 day after the preparation and in the week after the preparation of the sample to avoid its evolution. We prepare our dispersions by weighting a given amount of PVC particles, a given amount of DINCH. The solid fractions are then calculated knowing the density of PVC $\rho_{PVC} = 1.38\ g/cm^3$ and the density of DINCH $\rho_{Dinch} = 0.95 g/cm^3$. Suspensions are stirred 5 min at 1000 rpm using a Dispermat LC55 (VMA Getzmann) to ensure good dispersion state. This protocol was found to produce reproducible samples. The solid volume fraction of the suspension is defined as the volume of particles divided by the total volume: $\Phi = m_{PVC}/\rho_{PVC} + m_{Dinch}/\rho_{Dinch}$.

Cornstarch suspension

The cornstarch is supplied by Merck (CAS 9005-25-8) and used without further modification. It contains approximately 73% amylopectin and 27% amylose with a particle diameter of 14 μm (with a polydispersity of 40% as determined from static light scattering). Salt is used to match the density and to enhance the x-ray contrast. Dense cornstarch suspensions are obtained by dispersing 41 wt % of cornstarch at room temperature in a density-matched solvent composed of 46 wt % water and 54 wt % cesium chloride (CsCl).

Rheological procedure

Polyvinyl chloride

We used three geometries to measure the rheological behavior of PVC. In Fig. 1, we displayed the data measured in a homemade Couette cell with a rotor radius equal to 28 mm and a gap equal to 1.2 mm. The experiments have been performed using a Kinexus rheometer from Malvern and an ARG2 rheometrer from TA Instruments. The PVC sample is loaded in the Couette cell, and we set the geometry in the desired position and wait 60 s before starting the experiments. The first set of measurements has been obtained under constant imposed stress ramped up from 1 to 500 Pa in 36 logarithmically spaced steps of 60 s. The second set of measurements is different. The PVC sample is loaded in the Couette cell, and we set the geometry in the desired position and wait 10 min before starting the experiments. We applied a given shear

stress for 1 hour and recorded the temporal evolution of the shear rate. At the end of the experiment, we discard the sample and start with a fresh one to study another shear stress. We have measured the lateral stiffness of the rotor of the Kinexus rheometer, by measuring the force exerted to move the rotor with a rigid tip of small contact area positioned at the top of the rotor. This stiffness is equal to $1.3 \times 10^4\ \mathrm{Nm}^{-1}$. Data of Fig. 3 have been collected in a Couette cell devoted to x-ray scattering with a rotor radius equal to 24 mm and a gap equal to 1 mm. The experiments have been performed using an ARG2 from TA Instruments. In this situation, the PVC sample is loaded in the Couette cell, and we set the geometry at the desired position and wait 60 s before starting the experiments. We apply steps of shear stress over 600 s. The various shear stresses applied are 5, 20, 50, 75, 100, 125, 150, 200, 300, 400, 200, and 50 Pa. We have measured the lateral stiffness of the rotor of the ARG2, by measuring the force exerted to move the rotor with a rigid tip of small contact area positioned at the top of the rotor. This stiffness is equal to $1.5 \times 10^4\ \mathrm{Nm}^{-1}$.

In the Supplementary Materials, we display data obtained in a cone-and-plate geometry of 2° angle and 40-mm radius using an ARG2 rheometer from TA Instruments. The geometry is sandblasted. The rheological procedure is the following. The PVC sample is loaded in the cone-and-plate geometry, and we set the geometry in the desired position and wait 10 min before starting the experiments. We applied a given shear stress for 1 hour and recorded the temporal evolution of the shear rate. At the end of the experiment, we discard the sample and start with a fresh one to study another shear stress. Let us underline that no wall slip was measured in these experiments. This was checked directly by measuring velocity profiles using ultrasound in Couette cells and indirectly by changing the gap size of a Couette cell.

Cornstarch

Contrary to PVC suspension, cornstarch suspensions display slip at the wall. We used two geometries to measure the rheological behavior of cornstarch suspensions: a smooth one and a rough one. The procedure applied for the smooth geometry is the following. The sample is loaded in a smooth Couette cell, which has a rotor radius of 24.5 mm and a gap of 0.5 mm, and a series of constant shear stresses are applied for 50 s. The applied values are 0.3, 1, 2, 3, 5, 8, 10, 12, 15, 20, 25, 30, 40, and 60 Pa. The experiments are performed using an ARG2 rheometer from TA Instruments. The duration of the steps is reduced compared to PVC to avoid evaporation. For this purpose, we also use a dedicated cover fixed at the top of the Couette cell. The procedure applied for the rough geometry is the following. The Couette cell has a rotor radius of 23.5 mm and a gap of 1.5 mm and a characteristic roughness of ~20 μm. The rheological procedure is the following. After loading the sample, a series of constant shear stresses are applied for 50 s. The applied values are 0.3, 1, 3, 6, 10, 12, 15, 20, 21, 25, 30, 40, 60, 100, and 200 Pa. The experiments are performed using an ARG2 rheometer from TA instrument. The duration of the steps is reduced compared to PVC to avoid evaporation. For this purpose, we also use a dedicated cover fixed at the top of the Couette cell.

SUPPLEMENTARY MATERIALS

Supplementary material for this article is available at http://advances.sciencemag.org/cgi/content/full/6/16/eaay5589/DC1

View/request a protocol for this paper from *Bio-protocol*.

REFERENCES AND NOTES

1. R. G. Larson, *The Structure and Rheology Of Complex Fluids (Topics in Chemical Engineering)* (Oxford Univ. Press, 1999).
2. N. J. Wagner, J. F. Brady, Shear thickening in colloidal dispersions. *Phys. Today* **62**, 27–32 (2009).
3. E. Brown, N. A. Forman, C. S. Orellana, H. Zhang, B. W. Maynor, D. E. Betts, J. M. DeSimone, H. M. Jaeger, Generality of shear thickening in dense suspensions. *Nat. Mater.* **9**, 220–224 (2010).
4. A. P. Gast, W. B. Russel, Simple ordering in complex fluids. *Phys. Today* **51**, 24–30 (1998).
5. T. Divoux, M. A. Fardin, S. Manneville, S. Lerouge, Shear banding of complex fluids. *Annu. Rev. Fluid Mech.* **48**, 81–103 (2016).
6. P. Coussot, Rheophysics of pastes: A review of microscopic modelling approaches. *Soft Matter* **3**, 528–540 (2007).
7. J.-F. Berret, D. C. Roux, G. Porte, Isotropic-to-nematic transition in wormlike micelles under shear. *J. Phys. II* **4**, 1261–1279 (1994).
8. J.-B. Salmon, A. Colin, S. Manneville, F. Molino, Velocity profiles in shear-banding wormlike micelles. *Phys. Rev. Lett.* **90**, 228303 (2003).
9. M. A. Fardin, D. Lopez, J. Croso, G. Grégoire, O. Cardoso, G. H. McKinley, S. Lerouge, Elastic turbulence in shear banding wormlike micelles. *Phys. Rev. Lett.* **104**, 178303 (2010).
10. C. Heussinger, Shear thickening in granular suspensions: Interparticle friction and dynamically correlated clusters. *Phys. Rev. E* **88**, 050201 (2013).
11. R. Seto, R. Mari, J. F. Morris, M. M. Denn, Discontinuous shear thickening of frictional hard-sphere suspensions. *Phys. Rev. Lett.* **11**, 218301 (2013).
12. M. Wyart, M. E. Cates, Discontinuous shear thickening without inertia in dense non-Brownian suspensions. *Phys. Rev. Lett.* **112**, 098302 (2014).
13. R. Mari, R. Seto, J. F. Morris, M. M. Denn, Shear thickening, frictionless and frictional rheologies in non-Brownian suspensions. *J. Rheol.* **58**, 1693–1724 (2014).
14. N. Y. C. Lin, B. M. Guy, M. Hermes, C. Ness, J. Sun, W. C. K. Poon, I. Cohen, Hydrodynamic and contact contributions to continuous shear thickening in colloidal suspensions. *Phys. Rev. Lett.* **115**, 228304 (2015).
15. J. R. Royer, D. L. Blair, S. D. Hudson, Rheological signature of frictional interactions in shear thickening suspensions. *Phys. Rev. Lett.* **116**, 188301 (2016).
16. S.-I. Nagahiro, H. Nakanishi, Negative pressure in shear thickening band of a dilatant fluid. *Phys. Rev. E* **94**, 062614 (2016).
17. J. Comtet, G. Chatté, A. Niguès, L. Bocquet, A. Siria, A. Colin, Pairwise frictional profile between particles determines discontinuous shear thickening transition in non-colloidal suspensions. *Nat. Commun.* **8**, 15633 (2017).
18. C. Clavaud, A. Bérut, B. Metzger, Y. Forterre, Revealing the frictional transition in shear-thickening suspensions. *Proc. Natl. Acad. Sci. U.S.A.* **114**, 5147–5152 (2017).
19. M. Hermes, B. M. Guy, W. C. K. Poon, G. Poy, M. E. Cates, M. Wyart, Unsteady flow and particle migration in dense, non-Brownian suspensions. *J. Rheol.* **60**, 905–916 (2016).
20. R. N. Chacko, R. Mari, M. E. Cates, S. M. Fielding, Dynamic vorticity banding in discontinuously shear thickening suspensions. *Phys. Rev. Lett.* **121**, 108003 (2018).
21. V. Rathee, D. L. Blair, J. S. Urbach, Localized stress fluctuations drive shear thickening in dense suspensions. *Proc. Natl. Acad. Sci. U.S.A.* **114**, 8740–8745 (2017).
22. B. Saint-Michel, T. Gibaud, S. Manneville, Uncovering instabilities in the spatiotemporal dynamics of a shear-thickening cornstarch suspension. *Phys. Rev. X* **8**, 03100 (2018).
23. M. Gholami, A. Rashedi, N. Lenoir, D. Hautemayou, G. Ovarlez, S. Hormozi, Time-resolved 2D concentration maps in flowing suspensions using X-ray. *J. Rheol.* **62**, 955–974 (2018).
24. A. Fall, F. Bertrand, D. Hautemayou, C. Mezière, P. Moucheront, A. Lemaître, G. Ovarlez, Macroscopic discontinuous shear thickening versus local shear jamming in cornstarch. *Phys. Rev. Lett.* **114**, 098301 (2015).
25. A. Fall, F. Bertrand, G. Ovarlez, D. Bonn, Shear thickening of cornstarch suspensions. *J. Rheol.* **56**, 575–591 (2012).
26. R. L. Hoffman, Discontinuous and dilatant viscosity behavior in concentrated suspensions. I. Observation of a flow instability. *Trans. Soc. Rheol.* **16**, 155–173 (1972).
27. G. Chatté, J. Comtet, A. Niguès, L. Bocquet, A. Siria, G. Ducouret, F. Lequeux, N. Lenoir, G. Ovarlez, A. Colin, Shear thinning in non-Brownian suspensions. *Soft Matter.* **14**, 879–893 (2018).
28. S. Jack Willey, C. W. Macosko, Steady shear rheological behavior of pvc plastisols. *J. Rheol.* **22**, 525–545 (1978).
29. I. M. Krieger, Rheology of monodisperse latices. *Adv. Colloid Interface Sci.* **3**, 111–136 (1972).
30. B. J. Maranzano, N. J. Wagner, The effects of particle size on reversible shear thickening of concentrated colloidal dispersions. *J. Chem. Phys.* **114**, 10514–10527 (2001).
31. G. Bossis, P. Boustingorry, Y. Grasselli, A. Meunier, R. Morini, A. Zubarev, O. Volkova, Discontinuous shear thickening in the presence of polymers adsorbed on the surface of calcium carbonate particles. *Rheol. Acta* **6**, 415–430 (2017).
32. R. J. Larsen, J.-W. Kim, C. F. Zukoski, D. A. Weitz, Fluctuations in flow produced by competition between apparent wall slip and dilatancy. *Rheol. Acta* **53**, 333–347 (2014).
33. A. Fall, A. Lemaître, F. Bertrand, D. Bonn, G. Ovarlez, Shear thickening and migration in granular suspensions. *Phys. Rev. Lett.* **105**, 268303 (2010).
34. S. Garland, G. Gauthier, J. Martin, J. F. Morris, Normal stress measurements in sheared non-Brownian suspensions. *J. Rheol.* **57**, 71–88 (2013).

35. L. O. Gálvez, S. de Beer, D. van der Meer, A. Pons, Dramatic effect of fluid chemistry on cornstarch suspensions: Linking particle interactions to macroscopic rheology. *Phys. Rev. E* **95**, 030602 (2017).
36. H. M. Laun, Normal stresses in extremely shear thickening polymer dispersions. *J. Nonnewton. Fluid Mech.* **54**, 87–108 (1994).
37. D. Lootens, H. Van Damme, P. Hébraud, Giant stress fluctuations at the jamming transition. *Phys. Rev. Lett.* **90**, 178301 (2003).
38. A. Singh, R. Mari, M. M. Denn, J. F. Morris, A constitutive model for simple shear of dense frictional suspensions. *J. Rheol.* **62**, 457–468 (2018).
39. N. J. Balmforth, J. W. M. Bush, R. V. Craster, Roll waves on flowing cornstarch suspensions. *Phys. Lett. A* **338**, 479–484 (2005).
40. N. Y. C. Lin, C. Ness, M. E. Cates, J. Sun, I. Cohen, Tunable shear thickening in suspensions. *Proc. Natl. Acad. Sci. U.S.A.* **113**, 10774–10778 (2016).

Acknowledgments: We thank all the people of the program Physics of Dense Suspensions at Kavli Institute of Theoretical Physics. Access to the x-ray device was provided by PLACAMAT, UMS3626-CNRS/University of Bordeaux. **Funding:** We acknowledge support from the Agence Nationale de la Recherche (Project Fluididense ANR-17-CE07-0040, Programme Investissement d'Avenir Labex, and Equipex Institut Pierre Gilles de Gennes). This research was supported in part by the NSF under grant no. NSF PHY17-48958. G.C. thanks Tarkett for financial support and raw materials related to the PhD project "Flow behaviour of concentrated PVC suspensions" led at ESPCI Paris (laboratory SIMM, CNRS UMR 7615) from September 2014 to September 2017 and thanks F. Lequeux for advice and supervision in this PhD project. W.J.S. acknowledges funding from the People Programme (Marie Curie Actions) of the European Union's Seventh Framework Programme (FP7/2007-2013) under REA grant agreement n. PCOFUND-GA-2013-609102 "Putting the double electrode at work," through the PRESTIGE programme coordinated by Campus France from October 2017 to December 2019. **Author contributions:** G.O. and A.C. contributed equally to the design of the study. G.C., A.V.N.L., A.F., W.J.S., A.C., and G.O performed the experiments. G.O., R.M., and A.C. analyzed the results. G.O., W.S., and A.C. wrote the paper. **Competing interests:** The authors declare that they have no competing interests. **Data and materials availability:** All data needed to evaluate the conclusions in the paper are present in the paper and/or the Supplementary Materials. Additional data related to this paper may be requested from the authors.

Submitted 4 July 2019
Accepted 24 January 2020
Published 17 April 2020
10.1126/sciadv.aay5589

Citation: G. Ovarlez, A. Vu Nguyen Le, W. J. Smit, A. Fall, R. Mari, G. Chatté, A. Colin, Density waves in shear-thickening suspensions. *Sci. Adv.* **6**, eaay5589 (2020).

Science Advances

Density waves in shear-thickening suspensions

Guillaume Ovarlez, Anh Vu Nguyen Le, Wilbert J. Smit, Abdoulaye Fall, Romain Mari, Guillaume Chatté and Annie Colin

Sci Adv **6** (16), eaay5589.
DOI: 10.1126/sciadv.aay5589